Pergamon

Cement and Concrete Research, Vol. 27, No. 10, pp. 1501–1511, 1997

0008-8846/97 $17.00 + .00

PII S0008-8846(97)00169-5

# SIMILARITIES AND DIFFERENCES OF MICROSTRUCTURE AND MACRO PROPERTIES BETWEEN PORTLAND AND BLENDED CEMENT

**W. Jiang, M.R. Silsbee, and D.M. Roy**
Intercollege Materials Research Laboratory, Pennsylvania State University, University Park, PA 16802

(Refereed)
(Received March 21, 1997; in final form May 15, 1997)

## ABSTRACT

The relationship between microstructure and macro properties of different cementitious materials has been investigated. This study consists of the following tasks: using NMR and IR to better characterize the amorphous and poorly crystalline phases that occur in blended cements; characterizing the microstructure of the hydration products of modified Portland cement as a function of different percentages of pozzolan replacements by ESEM, SEM, and EDS; comparing the properties of blended cement pastes with a control group of normal Portland cements; and studying the engineering aspects of blended cement that are important for identifying and characterizing fundamental phenomena that are responsible for their durability. The overall influence of the nanoscale and microscale structure of blended and Portland cement on the properties of the resultant composite will be discussed. © *1997 Elsevier Science Ltd*

## Introduction

Blended cements have attracted intensive attention (1). In the past, there have been many successful practices of blended cement in the concrete industry. This study addresses three important roles in advancing the use of blended components: 1) incorporating those components into more products and processes, 2) modifying products to augment their compatibility with engineering properties, and 3) optimizing cement and concrete systems by optimizing resistance to chemical attack, freezing/thawing, and repressing alkali-aggregate-reaction. There is a significant pool of knowledge to draw from in order to optimize the use of slags and fly ashes to produce concretes with properties equal to, or better than, those using 100% ordinary Portland cement (OPC) (2–5). Recently, the investigations of incorporating large volumes of blended components have attracted intensive research attention (6.7). ASTM C 1157 (8), "Standard Performance Specification for Blended Hydraulic Cement," offers greater flexibility than the earlier prescriptive standard, C595. Swamy, commenting on the European experience of utilizing fly ash and slag, pointed out that the need to correlate requirements for quality control and quality assurance with the real performance of the concrete in the structure cannot be overemphasized (9). There still is a necessity to describe the similarities and differences of microstructures and microproperties between Portland and blended cements using modern material science. This study has attempted to provide an

analysis of the different aspects of blended components and to identify the interventions and modifications that can improve the performance of the entire blended cement system.

## Experimental

### Starting Materials

Ordinary Portland cement (OPC), assigned Materials Research Laboratory code # I-35, was obtained from Keystone Cement Co. It has a density of 3.12 g/cm$^3$ and BET surface area of 0.88 m$^2$/g. The particle size distribution range, determined by using an X-ray sedimentation technique (Sedigraph) is 1.2–50 μm. The glassy blast furnace slag used in this study has a density of 2.95 g/cm$^3$ and BET surface area of 0.80 m$^2$/g. The particle size distribution range is 0.7–40 μm. Silica fume (SF) has a density of 2.05 g/cm$^3$ and surface area of 18.02 m$^2$/g. The particle size distribution range is 0.1–5.0 μm.

Pastes and mortars were first prepared by combining cement and mineral admixtures with water, mixing for 2 min, resting for 3 min, then again mixing for 2 min (2-3-2 mixing sequence).

TABLE 1
The chemical composition of Type I OPC (wt. %)

| Type I | Code# | $SiO_2$ | $Al_2O_3$ | CaO | $Fe_2O_3$ | MgO | $K_2O$ | $Na_2O$ | $SO_3$ | L.O.I. |
|---|---|---|---|---|---|---|---|---|---|---|
| OPC | I-35 | 20.30 | 5.67 | 60.43 | 6.23 | 3.14 | 0.90 | 0.36 | 2.8 | 2.8 |
| Slag | G-24 | 35.60 | 10.40 | 37.60 | 1.16 | 12.80 | 0.33 | 0.07 | 0.87 | 1.72 |
| Fly ash | G-07 | 51.95 | 27.54 | 5.60 | 7.75 | 1.59 | 1.43 | 0.56 | 1.36 | 1.83 |
| SF | G-15 | 95.90 | 0.52 | 0.20 | 0.05 | 0.18 | 0.40 | 0.12 | 0.10 | 2.90 |

TABLE 2
Density, surface area and particle size distribution data of starting materials

| Material | Density (g/cm$^3$) | Surface area (m$^2$/g) | Size distribution range (μm) |
|---|---|---|---|
| OPC (type I) | 3.12 | 0.85 | 1.1 – 50 |
| Class F Fly ash | 2.46 | 0.69 | 2.0 – 40 |
| Slag | 2.90 | 0.75 | 0.7 – 40 |
| Silica fume | 2.05 | 18.02 | 0.1 – 5.0 |

TABLE 3
Mixture proportions (by weight)

| Paste | Mortar |
|---|---|
| OPC (Type I cement) + deionized water at w/c = 0.22, 0.25, 0.3, 0.35, 0.4 | OPC:Sand (C 109 ASTM): 1.0:2.25 at w/c = 0.3, 0.35, 0.44 |
| Blended cement system | Blended cement system |
| Using slag, fly ash, or SF as replacements by cements wt% (5–100%) | Using slag, fly ash, or SF as replacements by cements wt% (5–100%) |
| Casting in ø1.25 in × 1.5 cylinders | Casting 2 in cubes |

## Characterization

*SEM-EDX.* An International Scientific Instruments ISI-DS 130 dual stage Scanning Electron Microscope (SEM) with a Kevex Energy Dispersive X-ray analyzer (EDX).

*Zeta-Potential.* Zeta-potentials of cement (in presence and absence of superplasticizer) was measured using a microelectrophoretic technique, that has been described in detail elsewhere (10).

*XRD.* Powder x-ray diffraction was performed on a Scintag Automated x-ray diffractometer (CuK$\alpha$ radiation, $\lambda$ = 1.540598Å) interfaced with a microVAX computer.

*TGA.* A Harrop Laboratories Thermogravimetric analyzer (TG 716) with a Cahn balance was used in this study.

*Isothermal Conduction Calorimeter.* A thermostatically controlled Haake F3 water circulator with heating and cooling equipment was used in conjunction with a Thermonetics Corporation calorimeter. In each case, 3 g of powder was placed in metal container, then 1.5 g of water was added.

*Pore Solution.* Samples of the aqueous phase in contact with alkali activated cement pastes were obtained by expression of the pore solution from hardened cement pastes under high pressures of 500 MPa at ages ranging from 15 min to 90 days.

*Chemical Analysis.* Cation concentrations were determined using a dc-plasma emission spectrometer (Spectrametrics Inc.). Anion concentrations were determined using an ion chromatograph (Dionex model 2010i).

*NMR.* $^{29}$Si and $^{27}$Al MAS-NMR Spectra were recorded using a JEOL FX-90 instrument with a multinuclear probe covering the range 2.8–36.2 MHz.

*Setting Time.* Setting time was measured by Vicat needle (ASTM C191).

## Results and Discussion

### Strength Development and Isothermal Calorimetry

Figure 1 gives isothermal calorimetry curves showing rates of heat evolution as functions of time for Portland cement and slag blended cements (50:50) at w/c = 0.5 during the first 24 h of hydration. The high hydration temperature was used to accelerate the hydration, illustrating that the slag hydration has been accelerated by the increase in temperature to the same extent as the Portland cement hydration. The strength development (shown in Fig. 2) of slag-cement mortar (ASTM C 109) followed the expected pattern: the early age strengths of blended cements (hydrated at 25°C) were lower than those of portland cement (4), whereas a strength increase was observed at longer time (28 days) for up to 30% slag.

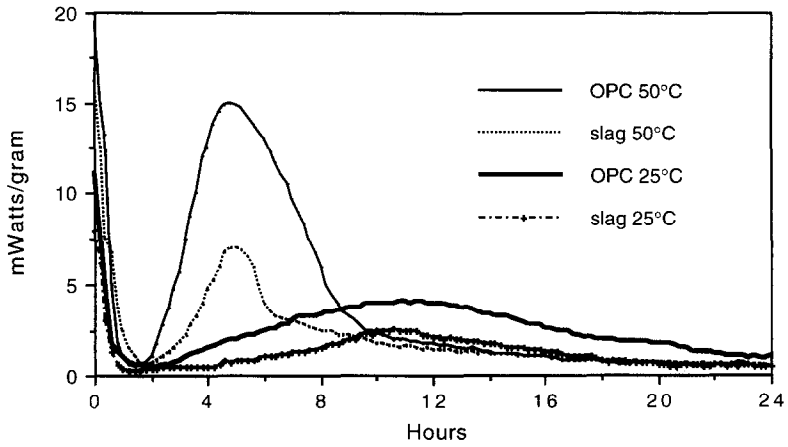


FIG. 1.
Calorimetric curves showing the rates of heat evolution as functions of time for Portland cement and slag (50:50%) at 25°C and 50°C during the first 24 h of hydration.

## Starting State and Mixing Effect

In describing the characteristics of blended components (slag as an example), basic crystal chemistry has been useful. It is beneficial to consider them from an atomistic point of view, defining as closely as possible the location of atoms relative to one another and the interaction between particles. This point of view leads to an understanding of structure and an insight into atomic interaction that is essential for developing models.

The high free energy of slags in a metastable glassy state generate a high driving force for reaction, a complex phenomena that we wish to understand. In Figure 3, the orginal x-ray "powder" diffraction pattern of glassy slag is very diffuse, consisting of broad humps, with

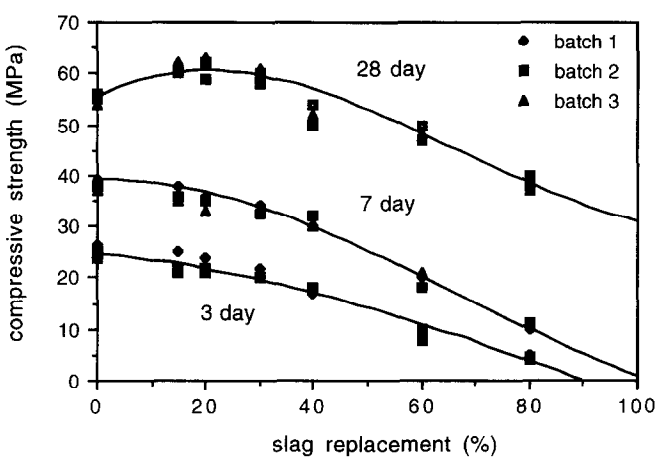


FIG. 2.
The effect of slag replacement on the compressive strength of blended cements curing at 25°C.

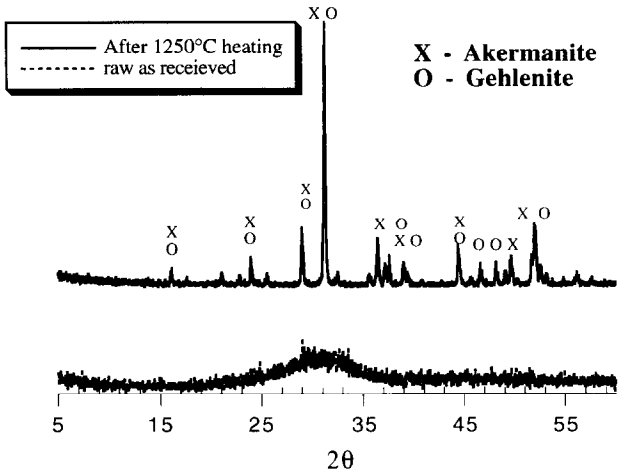


FIG. 3.
Powder X-ray diffraction patterns showing the crystalization of glassy slag to akermanite-gehlenite at temperatures of 1250°C.

only minor sharp peaks of crystalline material. The figure compares the x-ray powder diffraction pattern of the original glassy slag to the material found after heating at 1450°C for 30 min. After heating, the main crystalline phases were identified as akermanite (JCPD# 35-592) and gehlenite (JCPD# 35-755). The glass structures are typically short range order. Yasue et al. suggested that the blast furnace slag consisted of solid solution of akermanite ($Ca_2MgSi_2O_7$)-gehlenite ($Ca_2Al(SiAl)O_7$) (11).

There is diversity in the range of properties and applications of slags. The variability is due to differences in the inorganic components of the slag sources. The relationship of composition to hydraulicity and the relevance of the pozzolanic properties is various. Pozzolanic reactivity is a very important consideration for eventual applications in cement and concrete. Figure 4 shows the change in zeta potential of OPC and slag blended cements (50:50) as a result of superplasticizer adsorption, which were determined by the microelectrophoretic technique in the suspensions of 200 mg cement, slag, or fly ash in 100 ml deionized water. The superplasticizer is a surfactant that acts by the way of adsorption predominantly at the solid-water interface (12). Adsorption occurs via the polar backbone rather than the negatively charged end group, causing the highly charged end to be thrust towards the solution. In this way, cement grains and small particles acquire an increased negative charge—any entrained air will also be negatively charged—and hence the mixture becomes mutually repulsive. In deionzed water, the particles of OPC have positive potentials of about 5–10 mV (13), and slag and fly ash have negative potentials; these observations are consistent with early data (14–16).

## Hydration Patterns and Chemical Environment

Roy and Idorn (4) predicted that the role of alkali deserves greater attention in view of the findings that alkalis are slag-activators and that slag-cement concrete has proven effective in preventing alkali-silica reactions. It is noted that, until recently, it was widely believed that

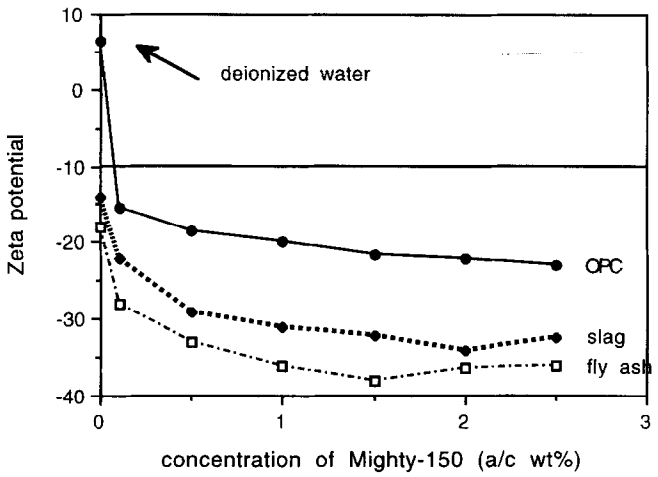


FIG. 4.
Zeta-potential of cement at different concentrations of superplasticizer.

the alkality of cement pore solution was controlled by its solubility. Immediately on mixing cement with water, its pH becomes strongly alkaline (17). Figure 5 shows that alkali level of slag cement in pore solution is lower than those of OPC. The OPC data used for comparsion was reported by Silsbee et al. (18). Figure 6 shows the SEM microstructure of hardened hydrated OPC paste and alkali activated slag. The two kinds of hydration product images reflects the difference. The SEM samples prepared were carefully treated. Microstructure is considered to be a key to performance (19–21). Roy et al. suggested that high-performance concrete possessed superior microstructure (21–23).

## $^{29}$Si and $^{27}$Al MAS-NMR

Figure 7 shows $^{29}$Si MAS-NMR spectra of OPC and slag. Pietersen, et al. (24) observed that blended cement with 70% slag has a chemical shift to −73 ppm (20). This study used $^{29}$Si

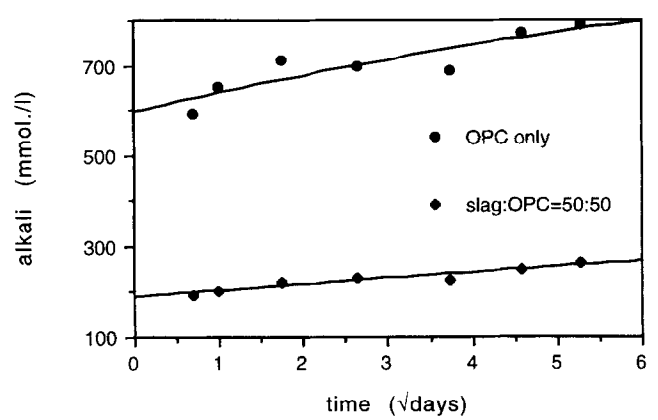


FIG. 5.
Alkali levels in a pore solution curing at 25°C.

(A)

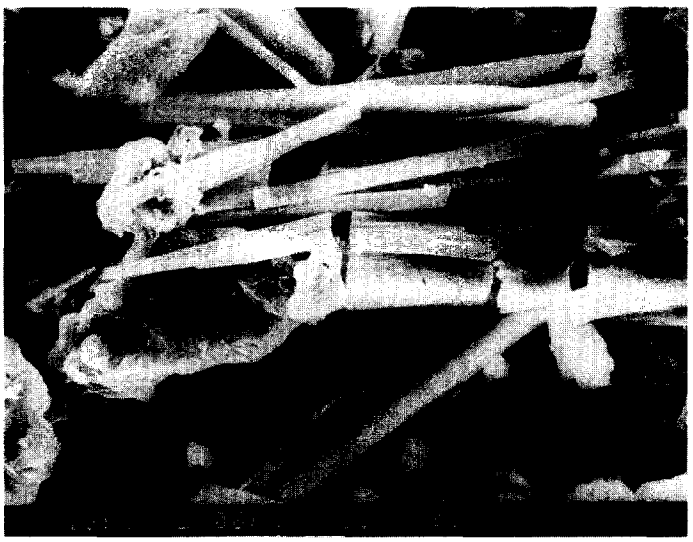

(B)

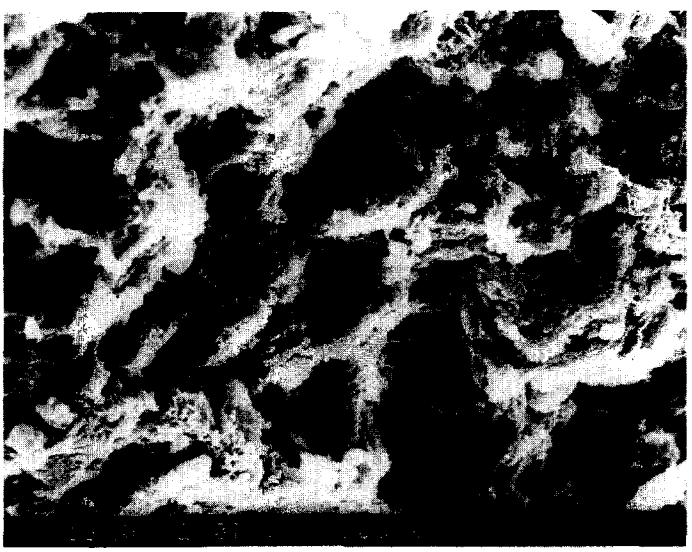

FIG. 6.
Micrograph of SEM of OPC (*A*) and slag cement paste (*B*) after 28 days hydration.

NMR on blast-furnace slag in order to better characterize the amorphous and poorly crystalline phases that occur in this system. The unreacted glass has a mainly dimeric silicate structure represented by a broad $^{29}Si$ peak centered at $-73.0$ and $-75.2$ ppm, with aluminum present exclusively in tetrahedral coordination. The alite starting materials used for comparison were provided by Kwan (25). The MAS-NMR spectrum shows that the alite consists of five $Q^0$ peaks (individual $SiO_4$ tetrahedras) ranging from approximately $-69$ to $-74$ ppm. These overlapping peaks can be distinguished by various shoulders on the major peaks

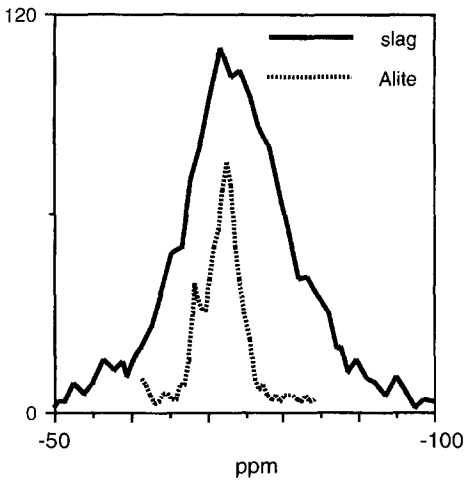


FIG. 7.
$^{29}$Si MAS-NMR spectra of OPC and slag ppm from TMS.

centered on approximately −73 ppm. Figure 8 shows the $^{27}$Al MAS-NMR spectra of slag and A-C-S-H (20% wt. % aluminum substituted C-S-H phases). The unreacted glass has a mainly aluminum structure represented by a broad $^{27}$Al peak centered at −61.2 ppm. Aluminum atoms are in tetrahedral coordination (fourfold = approximately 60 ppm) and octahedral coordination (sixfold = approximately 10 ppm).

## DTG

Figure 9 shows derivative thermogravimetric curves of OPC and blended slag cement after hydration for 7 days. The curves show two minima; the minimum at 110°C is broad. A

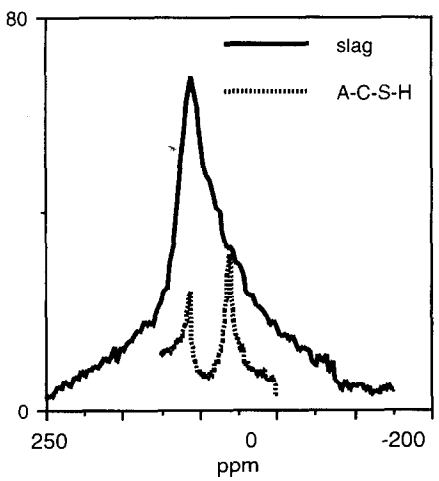


FIG. 8.
$^{27}$Al MAS-NMR spectra of slag and A-C-S-H ppm from $Al(H_2O)_6^{+3}$.

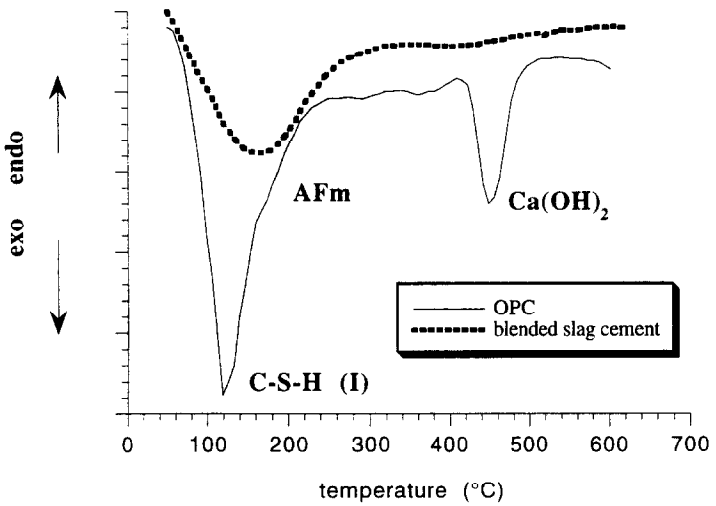


FIG. 9.
TGA data for OPC and blended slag cement (slag:OPC = 50:50) after hydration for 7 days.

comparison of the DTG curves of OPC and blended slag cement suggests that it is due to capillary water, and the second minmum, 420–480°C, is due to portlandite.

### Feature of Durability

It has been recognized for a long time that the use of pozzolana improves the durability of concrete (26). Hydration of OPC and blended cements may simply be divided into two basic modes: hydraulic reaction and pozzolanic reaction. The two reaction modes produce two basic hydration products, C-S-H and C-(N,K)-S-H, which, used by Roy and Idorn (4), still makes sense, and were documented in recent literature (22,28–35). Massazza (3) concluded that pozzolanic cements find their best applications when durability is a priority requirement. In such applications, a high resistance to chemical attack, freezing/thawing, and repressing alkali-aggregate-reaction are of concern. As a result, there is very convincing evidence to draw from in order to optimize the use of blended cements to produce concretes with properties equal to, or better than, those using 100% OPC. For all types of chemical attack, there is evidence that dispersed mineral addition may not only influence the perviousness of concrete but can also interfere with chemical reactions during hydration and in the corrosion. The photos shown in Figure 10 were assessed upon sulphate attack after immersion in 10% $MgSO_4$ solution for six months. In a series of mortars at w/c = 0.42, the mix proportion were: cement: ASTM standard sand (ASTM C 109):1:2.75. The blended cement provides considerable protection.

## Conclusions

Differences between the OPC and their blended components are evident; similarities permit the use of blended cements in "normal" concrete. Analysis of data from XRD, TGA, calorimetry, zeta-potential, IR, and NMR show that they are very consistent with the changes

(A) (B)

FIG. 10.
Photo of OPC (*A*) and slag blended cement (*B*) at slag:OPC = 50:50, after being immersed in 10% $MgSO_4$ solution for 6 months.

in composition. Results indicated that although the dominant hydration product in both blended systems and OPC is C-S-H, there is a difference in quantity, quality, and microstructure of the final products. This study reflects the strong contribution of blended cement components to the durability of the hydration products.

## Acknowledgment

This research was partly supported by the National Science Foundation grant MSS-9123239.

## References

1. V.M. Malhotra and R.T. Hemmings, Cem. Concr. Compos. 17, 23–35 (1995).
2. E.W. Miller, Cem. Concr. Compos. 15, 185–214 (1993).
3. F. Massazza, Cem. Concr. Compos. 15, 185–214 (1993).
4. D.M. Roy and G.M. Idorn, ACI J. 79, 445–457 (1982).
5. D.M. Roy and R.I.A. Malek, Mineral Admixtures in Cement and Concrete S.N. Ghosh (ed), pp. 84–117, ABI Books Pvt. Ltd., New Delhi, India, 1993.
6. A. Bilodeau, V. Sivasundaram, K.E. Painter, and V.M. Malhotra, ACI Mater. J. 91, 3–12 (1994).
7. R.J. Detwiler, J. Rock Prod. July, 27–33 (1996).
8. ASTM, Annual Book of Standards, 04.01, 463–467 (1994).
9. R.N. Swamy, Mater. Struct. 26, 600–613 (1993).
10. R.I.A. Malek and D.M. Roy, Mater. Res. Soc. Symp. Proc. 289, 191–198 (1993).
11. T. Yasue, K. Tazaki, A. Kidera, and Y. Arai, Gypsum & Lime (in Japanese) 212, 3–10 (1988).
12. Hewlett and Young, J. Mater. Edu. 9, 395–435 (1987).
13. E. Nägele, Cem. Concr. Res. 16, 853–863 (1986).
14. P.J. Andersen and D.M. Roy, Cem. Concr. Res. 17, 805–813 (1987).

15. D.M. Roy and M. Daimon, 7th ICCC Paris II, 242–246 (1980).
16. R.I.A. Malek, M.R. Silsbee, and D.M. Roy, 8th ICCC Rio de Janeiro III, 270–275 (1986).
17. S. Tanaka, K. Inoue, Y. Shimoyama, and R. Tomita, ACI Mater. J. 92, 429–436 (1995).
18. M.R. Silsbee, R.I.A. Malek, and D.M. Roy, 8th ICCC Rio de Janeiro III, 263–269 (1986).
19. S.L. Marusin, J. Cem. Concr. Compos. 17, 311–318 (1995).
20. I.G. Richardson and G.W. Groves, J. Mater. Sci. 27, 6204–6212 (1992).
21. D.M. Roy, M.R. Silsbee, S. Sabol, and B.E. Scheetz, Transportation Research Record No. 1478, pp. 11–19, National Academy Press, Washington, D.C., 1995.
22. D.M. Roy, Proc. 3rd Int. Conf. on Fly Ash, Silica Fume, Slag & Other Mineral By-Products in Concrete, Montebello, V.M. Malhotra (ed.), ACI, SP-114, Detroit, MI, I, 117–138 (1989).
23. H. Uchikawa, S. Hanehara, and H. Hiro, Cem. Concr. Res. 26, 101–111 (1996).
24. H.S. Pietersen, Application of NMR Spectroscopy to Cement Science, P. Colombet and A. Grimmer (eds.), pp. 29–238, Gordon and Breach Science Publishers, Amsterdam, 1994.
25. S. Kwan, Structure and Phase Relations of Calcium Silicate Hydrate and Related Phases in the System: Calcium Oxide-Aluminum Oxide-Silcon Oxid-Water, Ph.D. Thesis, Pennsylvania State University, USA, 1995.
26. J. Kropp, Performance Criteria for Concrete Durability, J. Kropp and H.K. Hilsdorf (eds.), p. 85, E & FN SPON, London, 1995.
27. J.L. LaRosa and M.W. Grutzeck, Wld. Cem. November, 65–71 (1995).
28. W. Jiang, M.R. Silsbee, E. Breval, and D.M. Roy, Mechanisms of Degradation of Cement-Based Systems, K.L. Scrivener and J.F. Young (eds.), E & FN SPON/Chapman & Hall Publishers, London (in press).
29. H.F.W. Taylor, J. Advn. Cem. Bas. Mat. 1, 38–46 (1993).
30. A. Neville, J. Concr. Int. July, 32–33 (1994).
31. D.M. Roy and M.R. Silsbee, Mater. Res. Soc. Symp. Proc. 245, 153–164, (1992).
32. C. Jolicoeur, M.A. Simard, T.C. To, J. Sharman, R. Zamojska, M. Dupuis, N. Spiratos, E. Douglas, and V.M. Malhotra, Advances in Concrete Technology, V.M. Malhotra (ed.) pp. 71–502, Minister of Supply and Services Canada, Ottawa, 1992.
33. E. Ma, C. Liu, P.W. Brown, and S. Komarneni. Cem. Concr. Res. 25, 417–425 (1995).
34. H.M. Jennings and P.D. Tennis, J. Am. Ceram. Soc. 77, 3161–72 (1994).
35. H.F.W. Taylor, Cement Chemistry, Acadmic Press, p. 99, 1990.